IASS 2018 BOSTON, JULY 16-20
CREATIVITY IN STRUCTURAL DESIGN

Proceedings of the IASS Symposium 2018
Creativity in Structural Design
July 16-20, 2018, MIT, Boston, USA
Caitlin Mueller, Sigrid Adriaenssens (eds.)

Designing (for) Decay: Parametric Material Distribution for Hierarchical Dissociation of Water-based Biopolymer Composites

Yen-Ju T. TAI[a,1,2], Christoph BADER[a,1,3], Andrea S. LING[a,1,4], Jean DISSET[a], Barrak DARWEESH[a], Jorge DURO-ROYO [a], Josh VAN ZAK[a], Nicolas HOGAN[a], and Neri OXMAN[*]

*The Mediated Matter Group, MIT Media Lab, Department of Architecture and Urban Planning, Massachusetts Institute of Technology.
75 Amherst St. E14-433C, Cambridge, MA 02142, USA.
neri@mit.edu

[a]The Mediated Matter Group, MIT Media Lab, Department of Architecture and Urban Planning, Massachusetts Institute of Technology.

[1]First authors: [2]yjtai@mit.edu, [3]bader_ch@mit.edu, [4]asling@mit.edu

Abstract

We present a design-to-fabrication workflow enabling hierarchical dissociation of water-based biopolymer composites on architectural scales. We leverage a water-based fabrication platform enabling the production of large-scale, geometrically complex, structurally hierarchical, functionally graded, and environmentally responsive structures along with robotic material deposition of viscous water-based materials. The robotic fabrication of such materials enables the controllable dissociation of structures in water, where dissociation rates of digitally fabricated parts are functions of material density distributions across surface areas. We introduce a methodology for the design and digital fabrication of objects with locally controllable dissociation properties through the generation of two-dimensional patterns by custom toolpaths that enable differentiated material densities across multiple length scales, while maintaining smooth transitions imposed by the material and the fabrication system.

Keywords: Water-based materials, robotic additive manufacturing, form-finding, material modeling.

1. Introduction

Contemporary sustainable building practices are still largely based on an extractive view of resource consumption, where even "green" construction materials usually require high energy processes to be made usable and to be recycled for re-use. Materials such as concrete, glass, and steel are typically structurally sound and environmentally resistant, providing architecture with its *firmitas*. Yet these materials are often assembled together without consideration of either the lifespans of their assemblies or the long-term future of the components from which they are made. As the buildings become obsolete or when the structures fail, these constituent parts are left behind in landfills and take centuries to degrade. With the use of biologically derived materials in additive manufacturing, we present an approach towards an alternative model of material use, where both use and decay can be constructively programmed into the lifecycle of a structure.

Furthermore, although recent advances in additive manufacturing are challenging the way in which we can conceive of and make objects and structures, digital design processes are nevertheless largely confined to being an extension to mechanical tools developed in the Industrial Age, where artifacts are made to be materially and functionally homogeneous within single objects and typologies. Here, water-based dissociation, as a precursor to decay, can be designed as a function of material density distribution,

tuned, and graded across spatial and temporal scales; whereby a denser material distribution in a given spatial domain takes more time to dissociate in water. The distribution, in turn, can be templated according to various environmental or structural criteria.

The work presented herein offers a prototypical design-to-fabrication framework for water-based material. The toolpath generation workflow allows precise local and global control over distribution of water-based materials and their associated properties. By characterizing dissociation properties of these materials in relation to material density distributions, we arrive at a design space that allows user to create objects with predefined dissociative behavior, guided by extrinsic and intrinsic constraints.

2. Methods

2.1. Biopolymer Composites

The biopolymer-based materials used are biocompatible, dissociate in water, and have a much shorter decay timescale than many common synthetic polymers; thus, they can be used as a model material system for water-based dissociation. The composites are based on a chitosan-cellulose mix as the structural layer [1], which when deposited onto films, can provide varying amounts of tensile strength to the print, depending on the deposition volume. The substrate film consists of pectin with varying amounts of chitosan, which dictates surface texture, rigidity, stickiness, and solubility.

Chitosan is a deacetylated derivative of the natural polysaccharide chitin, which is the second most abundant biopolymer on the planet and is found in arthropod shells, fish scales, and fungal cells. The monomer is structurally similar to cellulose, the most abundant biopolymer on the planet. Cellulose is a polysaccharide that provides stiffness to plant cell walls. The cellulose we use is typically deployed in construction to reinforce concrete. When suspended in a hydrogel, chitosan will contract and curl as it dries; whereas, cellulose will add flexibility and stability to the composite during drying.

Pectin is a polysaccharide found in fruit skins and cores as well as in structural complexes of trunks and branches of trees. In solution, pectin forms a sticky hydrogel that absorbs water and sets when cooled. We use the elastic pectin film as a base for more rigid chitosan-cellulose lines because the dried pectin forms Van der Waals interactions with the overlying print that can resist chitosan's tendency to contract and curl when drying. Depending on the surface roughness and hydrophilicity of the film, resistance to such contraction can tension the films to create more rigid constructs.

Pectin base: We used a base film composition of 32% apple pectin (w/v) (VWR, Radnor, PA), 2% chitosan (w/v) (85% de-acetylated VWR, Radnor, PA), 2% glycerin (v/v), and 1% glacial acetic acid (v/v). Water is heated to 80^{o}C and glycerin is mixed in. Pectin is added slowly and mixed with a hand mixer. The chitosan is sifted in slowly and mixed with the hand mixer. The temperature of the solution is lowered to 37^{o}C, and acetic acid is added while using the hand mixer to homogenize the solution.

Chitosan-cellulose composite: We printed a structural layer of 7% chitosan (w/v), 3.5% glacial acetic acid (v/v), 45% cellulose fiber (v/v), and 0.7% glycerin (v/v). Water is heated to 78^{o}C, at which point chitosan powder is stirred in. The solution temperature is lowered to 37^{o}C, and acetic acid is added and mixed with a hand mixer. The solution gels to the consistency of thin honey, cellulose fiber is slowly sifted in to form an extremely viscous hydrogel, which is then homogenized with the hand mixer.

2.2. Fabrication Platform

Figure 1 Photographs of the fabrication system, consisting of a 6-axis ABB IRB 4600 robotic arm and a custom pneumatic extrusion end-effector, as well as a sample print pattern showing sub-millimeter resolution

We use a multi-axis robotic platform with a custom pneumatic extrusion system that is programmed with instruction-feed capabilities, as described in detail in [2] and [3]. Motion path, speed, nozzle size, air pressure, and distance from the substrate are computationally tailored to match material selection and toolpath design. Modulating these parameters enables the user to tune the distribution of water-based materials in 2.5 dimensions, down to sub-millimeter tolerances, which is correlated with the dissociation rate of the material.

2.3. Computational Framework

To facilitate the challenge of pneumatically extruding viscous materials to create large-scale, functionally graded structures, the proposed computational workflow contains four processes developed to translate inherited material and fabrication information and constraints to geometric descriptions and machine instructions. An overview of the workflow is provided in **Figure 2 (b)**, with pseudocode given in **Figure 2 (a)**.

First, attribute maps given by objective functions–e.g. dissociative, environmental, structural, and others–and target a target shape are provided as inputs. The target shape is then variably populated with points according to the provided maps. The density distribution of points is based on material density-to-functional performance relationships and computed by suitable dithering algorithms.

The collection of points corresponding to the desired density distribution is then connected with edges, based on Delaunay triangulation. Since it is guaranteed to generate a mesh with only triangular faces to cover any domain, a Delaunay triangulation is used as a starting point and an approximation to the point density distribution, as it is widely recognized to be the "archetypical nice triangulation" [4].

The triangulated mesh is then incrementally turned into a feature, or directionally aligned quadrangular mesh through a modified re-meshing approach, as described in [5]. The algorithm first gradually moves the vertices, and then iteratively converges the mesh to a quadrangular one by removing shared edges between pairs of triangular faces, in a heuristic selection approach. The edges are removed by an angle deviation criterion, which is measured by the minimum angle between the edge and the directions of the vector field, evaluated at the midpoint of that edge.

The directional alignment to fields such as principal stress or principal curvature patterns could help improve or induce desirable mechanical and structural performance [6]–[8]. In addition, because these vector fields will directly inform the alignment of the existing curve network, there is no need to undergo the cumbersome process of obtaining principal stress lines by post-rationalization of the field, or reparameterization of the underlying geometry [9], through which problematic singularities or discontinuities often occur, as Tam and Mueller [7] have presented in the analysis of popular conventional design packages such as Millipede [11] and Karamba [12]. In other words, the directional field will be utilized as a reference towards which the edges of the already obtained graph should shift, instead of directly materializing as a geometric object.

The advantages of obtaining a quadrangular mesh are twofold. On the one hand, a polygonal mesh consisting of quadrilateral faces could be aligned to the principal directions of the geometry, or a given directional field, better than one that is made out of triangular faces. On the other hand, it enables the generation of a dual graph that will always return vertices of valence four. Therefore, there exists an Euler path, which traverses the graph completely by visiting each edge of the graph only once [13][14]. **Figure 2 (c)** illustrates the sequence of traversal of the same graph shown in **(b)**.

A process that enables the creation of a graph that can be traversed through a single tour from any given material distribution maps is advantageous for fabrication platforms that deposit water-based viscous material along complex geometric patterns because it eliminates the need to go through multiple toolpaths to complete a given pattern design. Therefore, the production procedure avoids potentially pausing at undesirable locations within the underlying geometry and reduces jumps to the next toolpath in the midst of printing, where uncontrollable material deposition might occur.

Once the dual graph of the well aligned quadrangular mesh is produced, and its traversal thus guaranteed to be Eulerian, two post-processing steps are taken to further improve the quality of the toolpath. During the implementation of Hierholzer's or Fleury's algorithm, a heuristic is applied to measure and sort which edge is best to be traversed next. The cost value assigned to each edge that enables the heuristic search could be assigned by either the user, additional external mapping intrinsic to the graph pattern itself, or a weighted combination of multiple factors.

A meaningful cost function explored here is the local turning angle between the current edge and each potential next edge. A lower cost will be assigned to edges that continue the straight-line trajectory of the current edge. As such, regional smoothness of the toolpath could be effectively improved. The comparative result of graph traversals based on different algorithms tested is shown in **Figure 2 (d)**.

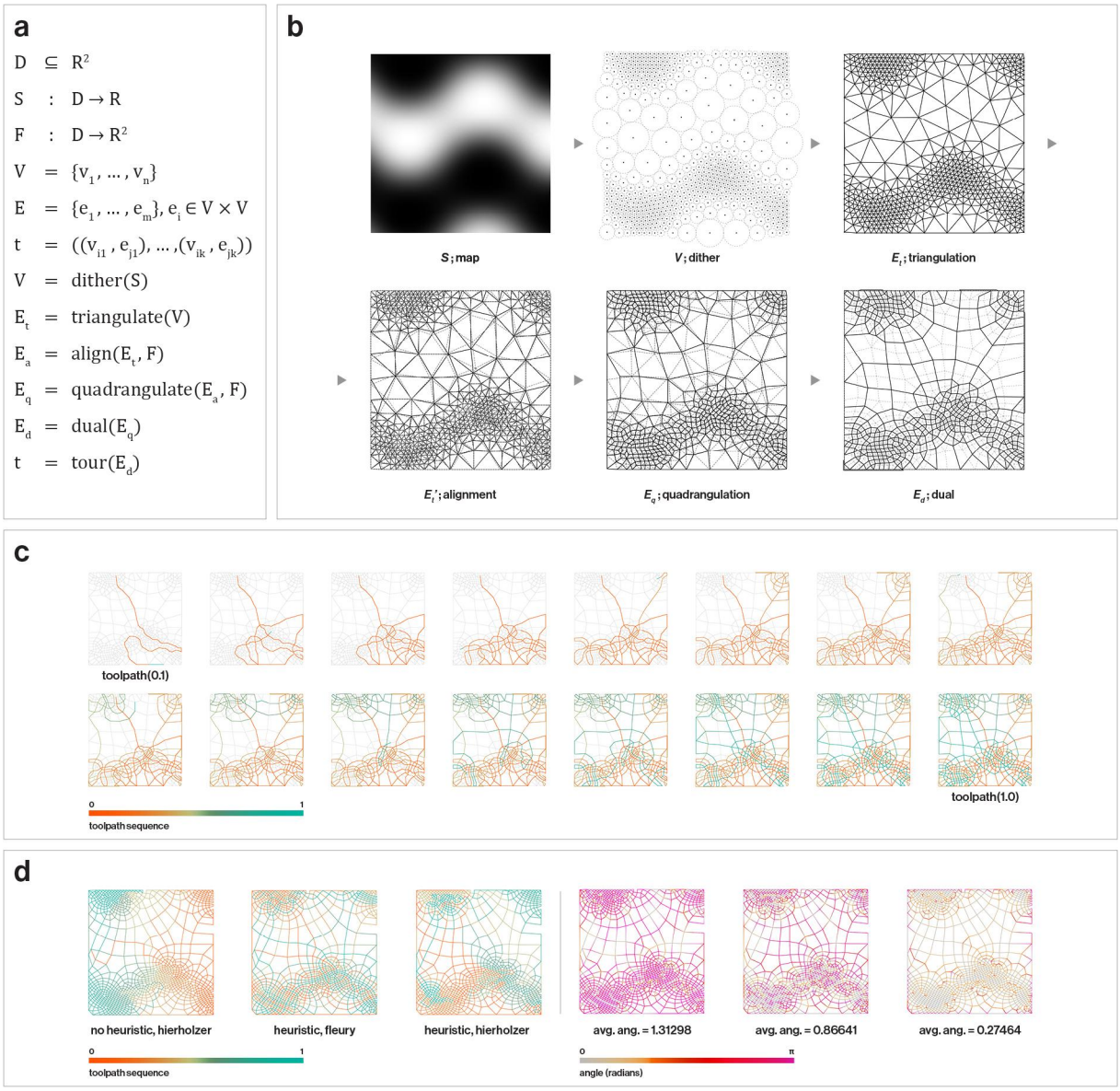

Figure 2 provides an overview of the computational workflow developed for the design and digital fabrication of viscous, water-based material through a material distribution modeling approach. (a) The pseudocode outlining the six main processes shown in (b)are mapping, dithering, triangulation, alignment, quadrangulation, and finding the dual graph. (c) The sequence of toolpath traversal of the obtained pattern-graph. (d) The three different algorithms tested for the heuristic search for best traversal sequence are analyzed. Average angle of the complete tour is used as a metric to measure how smooth a toolpath is; the lower the number, the better – indicating less turning overall.

3. Results

3.1. Characterization

Eight samples were printed in two sets of four 150 mm x 150 mm squares on an anodized aluminum substrate. The squares consisted of a base film of 35% pectin (w/v), 2% chitosan (w/v) mix. Approximately 75 mL of the pectin colloid was deposited in each square, with toolpath lines set in parallel, 3mm apart. The squares were left to air dry for 24 hours at room temperature and ambient humidity, after which the chitosan-cellulose toolpaths were applied.

The first set features four grids of different densities and different toolpath lengths, as shown in **Figure 3 (a)**. The grids were printed using three polylines, with all the parallel lines joined in one toolpath, and then a bounding box pass. Two layers of each polyline were printed at 40 PSI and speed of 5m per minute; the toolpath lengths were 45800 mm (1 mm spacing), 9800 mm (5 mm spacing), 3800 mm (15 mm spacing), and 2300 mm (30 mm spacing) long. The second set of toolpaths, shown in **Figure 3 (c)**, were based on the Euler path methodology, with mappings driven by the following sources for density distribution: a point source (4383 mm long), a line source (4459 mm long), a function source (in this case, a gyroid) (4489 mm long), and an image source (8526 mm long). The toolpaths were printed along one polyline, with an additional bounding box pass. Two layers of each polyline were printed at 40 PSI at 5m per minute.

All the samples were left to dry for 12 hours, before removal from the substrate. The panels were then set in shallow dishes of distilled water for 14 days, and the dissociation was monitored via time-lapse photography. The samples became saturated and expanded in volume, deforming with the expansion, after which the samples began to dissociate. The pectin film dissociated quickly in relation to the more viscous chitosan-cellulose layers. Mold growth began on Day 5. Photos at T_1=0 hr 0 min and T_2= 2 days 18 hr 18 min were analyzed to measure the amount of dissociation in relation to the material distribution. We use $m = \int |\nabla g|^2 dA$ (g is the greyscale value of the image) as a measure for how dissociated the pieces are in water. As $min \int |\nabla g|^2 dA$ implies $\nabla^2 g = 0$ whose solution g is a smooth as possible function suspect to boundary conditions. m indicates how blurred an image is, which we associate with dissociating. Thus, low values of m indicate high dissociation and conversely, high values indicate low dissociation.

Results are shown in **Figure 3 (e),** where measurements at two time-points, T_1=0 hr 0min, T_2= 2 days 18 hr 18 min, are analyzed. From the left graph we can see that the grid with a higher density of chitosan takes more time to dissociate. Similarly, on the right we see that material distributions with dense areas retain their shape and diffuse less. Furthermore, we can see that a uniform material distribution in the grid patterns results in dissociation graphs that have varying, yet similar, rates of dissociation, shifted proportionally with material density; despite having almost twice as much material as **b4**, **b3** shows a similar dissociation rate, but starting at a higher point in the graph. In contrast, the slopes of the dissociation graphs for variable density samples range considerably between samples, as the material distributions are not uniform within and across pieces. Although samples **d1**, **d2**, and **d3** received similar amounts of material depositions (similar toolpath lengths), **d3** dissociates at a much different rate than **d1** or **d2**. In addition, sample **d4** exhibits a much slower rate, indicating the distribution, with dense material bounding the perimeter of the sample, is more resistant to dissociation than the other three samples.

We reason that regardless of the amount of material, it is primarily the density distribution that affects the dissociation rate of these samples; while amounts of material distributed affect the total time for dissociation. Patterns with larger areas of densely patterned materials retain their shapes better and dissociate at a slower rate; while patterns with areas of sparse distribution that are not surrounded by denser regions exhibit larger deformation locally and faster global dissociation rates.

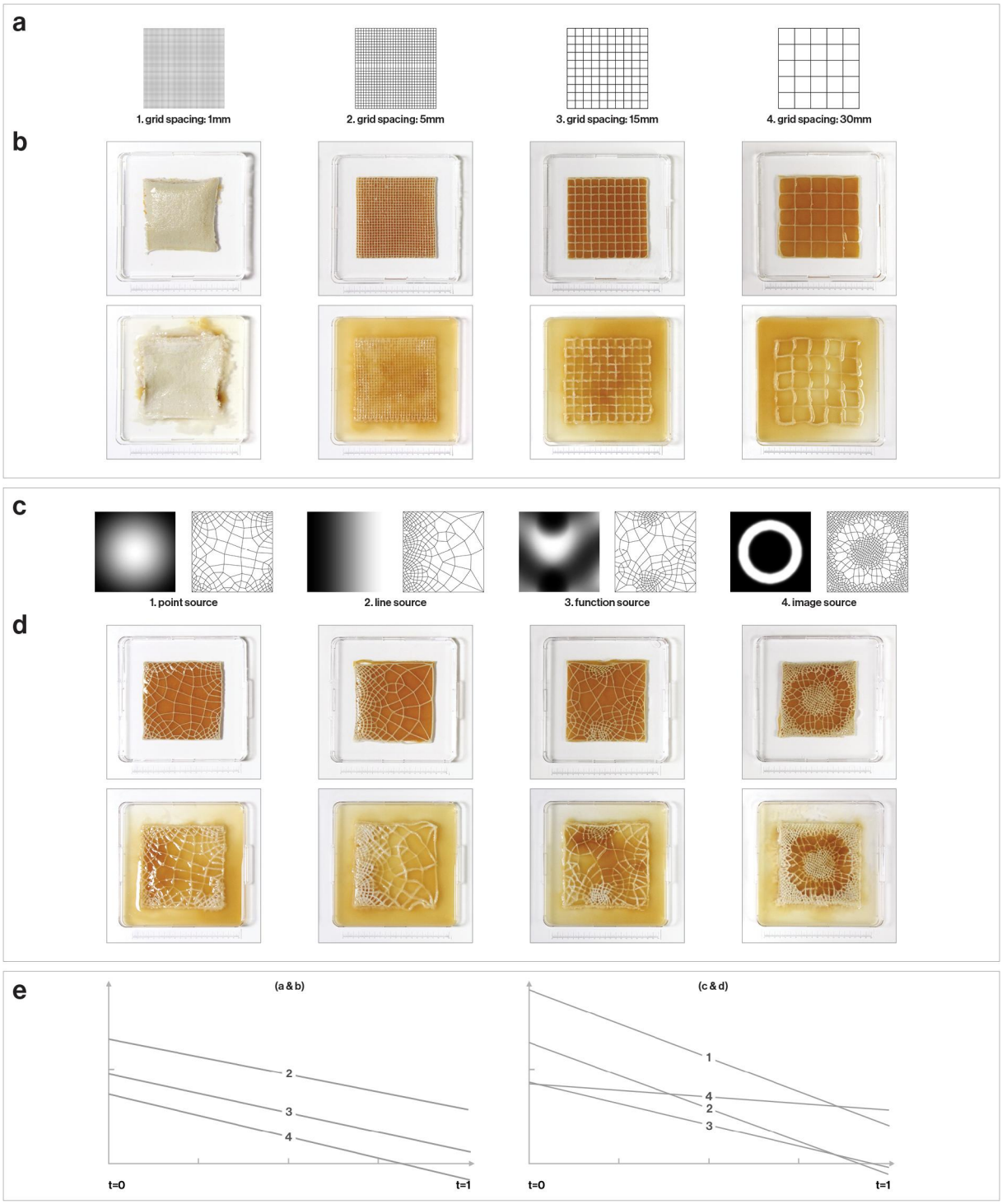

Figures 3 (a) and (c) illustrate the designed patterns of the two series of dissociation time-lapses shown in (b) and (d), respectively. (a) is a sequence of grids 3D printed at various spatial frequencies. From left to right: 1 mm, 5 mm, 15 mm, and 30 mm spacing, while (c) demonstrates that density could be templated through sources that are based on geometry -- here, a point source and line source function-based, and image-based. (e) illustrates the evaluation of the dissociation test. Areas with denser material distribution retain their shape and material concentration better; spatial distribution of material has effects on shape retention and degree of dissociation.

3.2. Simulation

We model the dissociation of biopolymer composites as highly viscous fluids. To do so, we use a fluid implicit particle schema [15], were initial viscosities are prescribed by material properties, and a heuristic viscosity falloff function is assigned to individual particles by material type (**Figure 4 (a)**). Dissociation in water is modeled by diffusion of water into materials (**Figure 4 (b))** and water content mapping by the respective falloff function in relation to viscosity. As water content increases throughout the substrate, viscosity decreases. Results for initial viscosity using a material distribution induced by a toolpath from Figure 3 are shown in **Figure 4 (c)**. From these figures, we see clear resemblance to the experiments shown in **Figure 3**.

Two additional conclusions can be drawn from the simulations. Firstly, dissociation is clearly related to geometric material deposition, as areas with more viscous materials dissociate slower. Secondly, dissociation behavior is also related to the material properties of the biopolymer composites -- specifically, their initial viscosity and its rate of change in water.

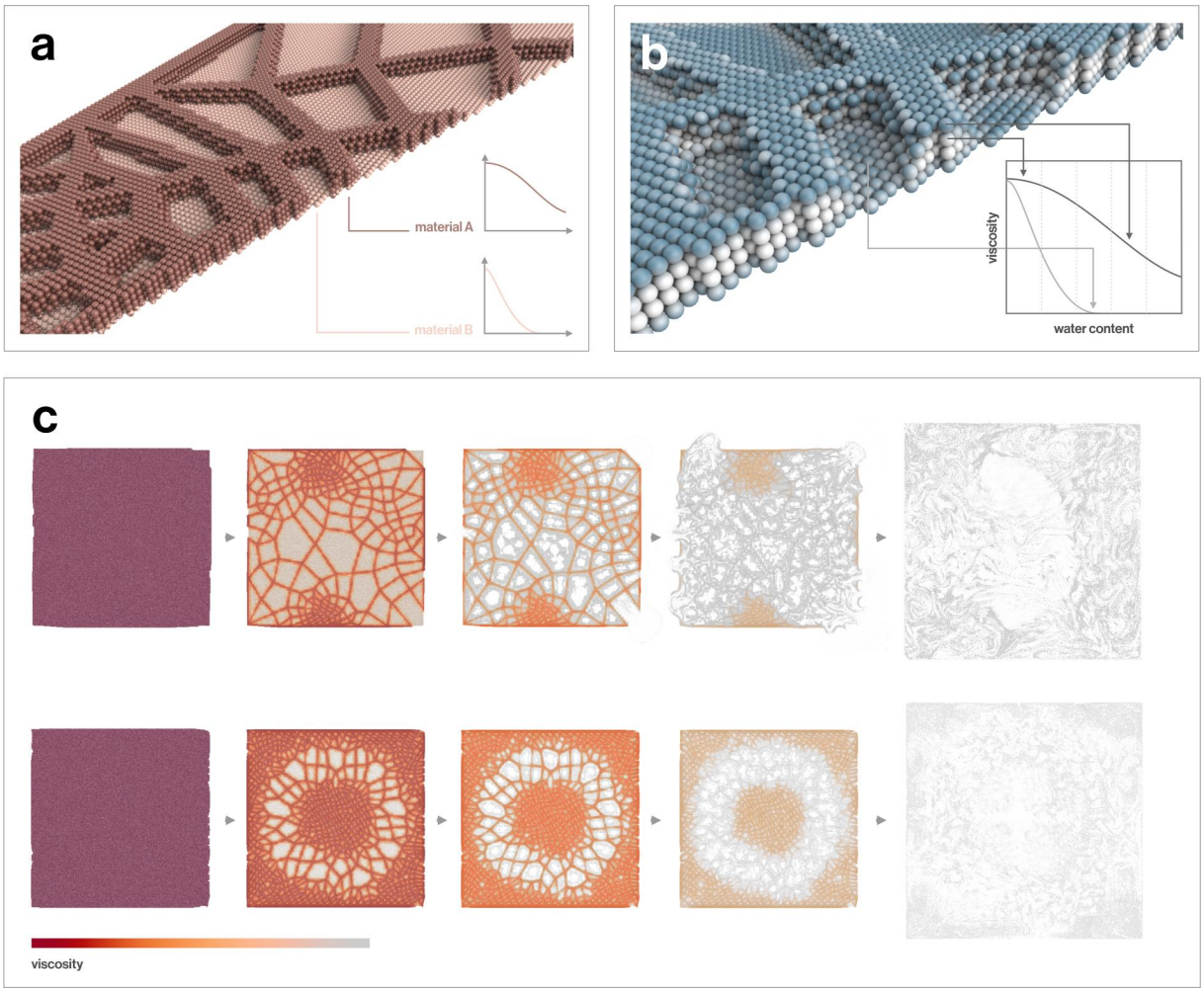

Figure 4: (a) Particles generated from cellulose-chitosan toolpaths with a pectin base layer. Viscosity falloff functions are assigned based on estimated material properties. (b) Diffusion of water into matter where water content is visualized in blue. (c) Dissociation simulations of two toolpaths used in previous experiments. We can observe fast dissociation of the composite in areas with low material deposition of the cellulose-chitosan, and vice-versa.

4. Conclusion

In this paper we presented an integrated framework for the design and digital fabrication of water-based biopolymer composites with controlled dissociation via tunable material distribution. We characterize the dissociation behavior of the produced composites with varying material distributions and present a

simulation framework for form-finding of dissociating structures. The work presented herein integrates a design methodology that emphasizes environmental conditions in a design paradigm that is primarily informed by structural considerations. Derived from organic matter, driven by environmental parameters, printed by robotic platforms, and shaped by water, this work points towards the possibility of fusing natural and manmade environments offering a new outlook on biologically-engineered and environmentally responsive design.

Acknowledgements

The authors would like to thank GETTYLAB for their support of this research, as well as the Autodesk BUILD Space.

References

[1] J. Van Zak, J. Duro-Royo, Y. T. Tai, A. S. Ling, C. Bader, and N. Oxman*, "Parametric Chemistry: Reverse Engineering Biomaterial Composites for Additive Manufacturing of Bio-cement Structures across Scales," *Towar. a Robot. Archit.*, 2018.

[2] J. Duro-Royo, L. Mogas-Soldevila, and N. Oxman, "Flow-based Fabrication: An Integrated Computation Workflow for Digital Design and Additive Manufacturing of Multi-functional Heterogeneously Structured Objects," *Comput. Des. J.*, 2015.

[3] J. Duro-Royo, L. Mogas-Soldevila, and N. Oxman, "Methods and Apparatus for Integrated Large Scale Robotic Fabrication of Functionally Graded Materials and Structures," 2014.

[4] J. A. Bærentzen, J. Gravesen, A. François, and A. Henrik, *Guide to Computational Geometry Processing*. Springer Science & Business Media, 2012.

[5] Y. Lai, L. Kobbelt, and S. Hu, "An Incremental Approach to Feature Aligned Quad Dominant Remeshing," *Proc. 2008 ACM Symp. Solid Phys. Model.*, vol. 1, no. 212, pp. 137–145, 2008.

[6] K.-M. M. Tam and C. T. Mueller, "Stress Line Generation for Structurally Performative Architectural Design," *Proc. 35th Annu. Conf. Assoc. Comput. Aided Des. Archit.*, pp. 94–109, 2015.

[7] P. Winslow, "Multi–criteria gridshell optimization: Structural lattices on freeform surfaces," in *Shell Structures for Architecture: Form Finding and Optimization*, vol. 9781315849, 2014, pp. 181–193.

[8] J. Fonseca, "The Loadpath - a way to understand the quality of structures," *J. Int. Assoc. Shell Spat. Struct.*, vol. 38, pp. 129–135, 1997.

[9] N. Ray, W. C. Li, B. Lévy, A. Sheffer, and P. Alliez, "Periodic global parameterization," *ACM Trans. Graph.*, vol. 25, no. 4, pp. 1460–1485, 2006.

[10] K.-M. M. Tam and C. T. Mueller, "Additive Manufacturing Along Principal Stress Lines," *3D Print. Addit. Manuf.*, vol. 4, no. 2, pp. 63–81, 2017.

[11] P. Michalatos and S. Kaijima, "Millipede," 2012.

[12] C. Preisinger and M. Heimrath, "Karamba - A toolkit for parametric structural design," *Struct. Eng. Int. J. Int. Assoc. Bridg. Struct. Eng.*, vol. 24, no. 2, pp. 217–221, 2014.

[13] C. Hierholzer and C. Wiener, "Ueber die Möglichkeit, einen Linienzug ohne Wiederholung und ohne Unterbrechung zu umfahren," *Math. Ann.*, vol. 6, no. 1, pp. 30–32, 1873.

[14] M. Fleury, "Deux problemes de geometrie de situation," *J. Math. Elem.*, vol. 2, no. 2, pp. 257–261, 1883.

[15] J. U. Brackbill, D. B. Kothe, and H. M. Ruppel, "Flip: A low-dissipation, particle-in-cell method for fluid flow," *Comput. Phys. Commun.*, vol. 48, no. 1, pp. 25–38, 1988.